Advanced Deep Learning Techniques for Industry 4.0: Application to Mechanical Design and Structural Health Monitoring

Fakhreddine Ababsa[a]
PIMM, Arts et Métiers ParisTech, CNRS, CNAM, HESAM University, Paris, France
Fakhreddine.ababsa@ensam.eu

Keywords: Generative Design, Deep Learning, Additive Manufacturing, Topology Optimization, Structural Health Monitoring (SHM), MLP, GAN.

Abstract: Nowadays, Deep Learning (DL) techniques are increasingly employed in industrial applications. This paper investigate the development of data-driven models for two use cases: Additive Manufacturing-driven Topology Optimization and Structural Health Monitoring (SHM). We first propose an original data-driven generative method that integrates the mechanical and geometrical constraints concurrently at the same conceptual level and generates a 2D design accordingly. In this way, it adapts the geometry of the design to the manufacturing criteria, allowing the designer better interpretation and avoiding being stuck in a time-consuming loop of drawing the CAD and testing its performance. On the other hand, SHM technique is dedicated to the continuous and non-invasive monitoring of structures integrity, ensuring safety and optimal performances through on-site real-time measurements. We propose in this work new ways of structuring data that increase the accuracy of data driven SHM algorithms and that are based on the physical knowledge related with the structure to be inspected. We focus our study on the damage classification step within the aeronautic context, where the primary objective is to distinguish between different damage types in composite plates. Experimental results are presented to demonstrate the effectiveness of the proposed approaches.

1 INTRODUCTION

Many industrial sectors have embraced the concepts and technologies of Industry 4.0. These technologies offer the opportunity to promote efficient, on-demand production through digitisation and the integration of intelligent machines. This transition is primarily driven by technological advances, which include artificial intelligence (AI) and machine learning, sensor networks, Internet of Things (IoT) technologies, cloud computing, additive manufacturing and the accessibility of large data sets that can be leveraged by these innovations. However, the degree of adoption of AI technologies for the industry 4.0 varies considerably from one industrial sector to another (Khelalef et al., 2019). Many research studies have been carried out last years on the use of AI in Industry 4.0. They highlight how the different AI technologies aim to solve problems concerning the acquisition, processing, modelling and interpretation of data results. For example, in (Nath et al., 2021) an AI-based feature engineering framework was introduced for rotor fault diagnosis. This study utilized a range of AI/ML methodologies to extract significant data features, enabling the detection of rotor faults. (Lockner et al., 2021) introduced an enhanced injection molding process through transfer learning. The authors employed neural networks and genetic algorithms to optimize the molding process, meeting customer demands for waste reduction and operational speed. In a study (Oehlmann et al., 2021), researchers employed an artificial neural network (ANN) to predict the pressure inside the nozzle of an FFF printer with the aim of optimizing the printing process. In (Mohan et al., 2021), a machine learning-based approach for predictive maintenance was proposed. They introduced a data-driven regression system to transition from Industry 3.0 to Industry 4.0 with minimal alterations to the existing setup. In another study (Arden et al., 2021), the necessity of implementing Industry 4.0 and AI-driven processes in the pharmaceutical sector was examined. They suggested that the pharmaceutical industry should

[a] https://orcid.org/ 0000-0003-3862-2449

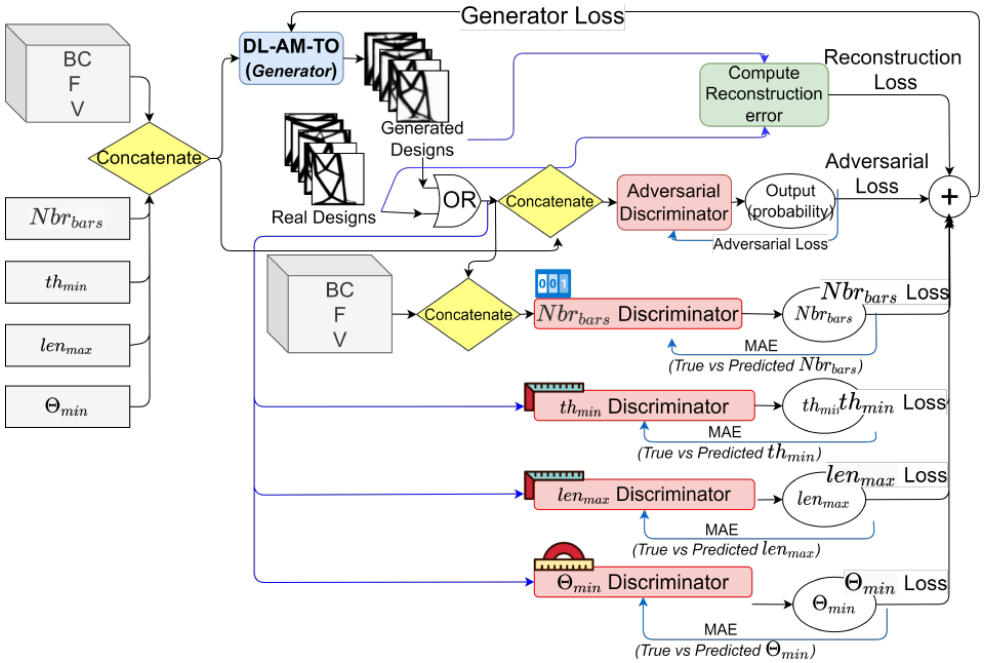

Figure 1: DL-AM-TO Training procedure.

leverage emerging cutting-edge technologies to transition into the next generation of manufacturing. In this paper, we aim to elaborate on two use cases of AI within the scope of Industry 4.0, offering a complementary perspective to the state of the art. The first case focuses on harnessing Generative Adversarial Networks (GANs) for design, optimization, and numerical validation in the field of additive manufacturing. The second case concerns the utilization of a Convolutional Neural Network (ConvNet) for the classification of damage cases in the context of Structural Health Monitoring (SHM) of aeronautical composite structures.

The rest of the manuscript is organized as follows: Section 2 describes the methodology proposed for the construction of the design algorithm using GAN's. Section 3 provides the details of the default classification method for SHM. Section 4 gives concluding remarks and suggestions for future work.

2 DL FOR ADDITIVE MANUFACTURING-DRIVEN TOPOLOGY OPTIMIZATION

In this work, we propose an advanced approach utilizing Deep Learning (DL) to incorporate not only mechanical constraints but also geometric constraints inherent to Additive Manufacturing (AM) at a conceptual level. DL's intrinsic capability to discern spatial correlations obviates the necessity for deriving explicit analytical formulas for geometric constraints, relying instead on the availability of a substantial dataset comprising numerous instances that encapsulate these constraints.

We propose a topological optimisation (TO) approach for data-driven AM (DLAM- TO). DL-AM-TO is a generative model that takes mechanical (Boundary conditions (BC), loads (F), and the volume fraction (V)) and geometrical conditions (the minimum thickness (th_{min}), the maximum length (len_{max}), the minimum overhang (θ_{min}), the number of bars (Nbr_{bars})) as inputs and generates a 2D structure following these constraints. It is trained within a five-discriminator-GAN (Goodfellow et al. 2014) framework consisting of a generator (DL-AM-TO) and five discriminators: the traditional adversarial discriminator and four geometric discriminators, a bar counter,th_{min}, len_{max} and θ_{min} predictors (Fig.1).

The four geometric constraints were chosen among the existing set of constraints as a use case to validate the proposed methodology.

2.1 Architecture

DL-AM-TO inherits the residual-convolutional encoder-decoder architecture (Zhang et al., 2018) presented in our previous work (Almasri et al., 2021)

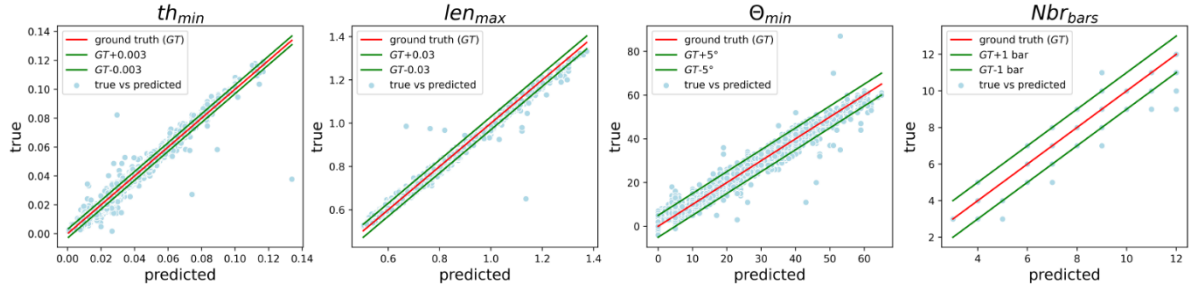

Figure 2: Performance of geometric discriminators showing predicted vs true values of th_{min}, len_{max}, θ_{min}, & Nbr_{bars}, from left to right respectively. The worst performant discriminator is clearly the th_{min}predictor.

with one difference; the skip-connections between the outputs of encoder layers and the inputs of decoder layers were eliminated here. The traditional discriminator consists of seven down-sample convolutional layers followed by a dropout and a final fully connected layer. The geometric discriminators' network consists of a stem, an Inception/Reduction Resnet-v1- block-A, an Inception/Reduction Resnet-v1-block-B, an Inception Resnet-v1-block-C followed by an average pooling layer, a dropout layer, and a fully connected layer1. We would like to point out that the input of the three geometric discriminators (th_{min}, len_{max} and θ_{min}) consists of the 2D design only, and the bar counter's input consists of the design alongside the mechanical conditions.

2.2 Training Loss Function

The most challenging aspect of GANs is to find an equilibrium between the generator and the discriminator and avoid the dominance of one over the other. The loss function with other training parameters play an important role into stabilizing the training and condemning the phenomenon of oscillating losses. In this work, the loss function is further challenging; it has to also account for the geometrical (th_{min}, len_{max}, θ_{min} and Nbr_{bars}) and mechanical (BC, F, V) constraints. Thus

$$L_G = \frac{1}{6}\left(L_r + \lambda_{adversial}\lambda_{adv} + L_{Nbr_{bars}} + L_{th_{min}} + L_{len_{max}} + L_{\theta_{min}}\right) \quad (1)$$

Where the reconstruction loss $L_r = \frac{1}{N}\sum_{i=1}^{N}(x_i - \hat{x}_i)^2$. x_i and $\hat{x}_i$ are the real and generated 2D design and N is the batch size, $L_c = \sum_{i=1}^{N}|c_i - \hat{c}_i|$, $c \in \{Nbr_{bars}, th_{min}, len_{max}, \theta_{min}\}$ c_i and $\hat{c}_i$ are the input and predicted geometrical values respectively, and L_{adv} is the Binary Cross Entropy ($0 \leq L_{adv} \leq 100$ in PyTorch). Hence, $L_{adversial}$ was set to *0.01*, so L_{adv} becomes of the same order of magnitude of all other losses varying between 0 and 1.

2.3 Results

In this section, we present the performance of DL-AM-TO with regard to geometric constraints. Thus, we not only evaluate the aesthetics of the generated designs (Fig. 2), but also test DL-AM-TO's ability to respond to geometric changes (Fig. 3).

2.3.1 Training and Test Dataset

11719 samples of GMCAD (Almasri et al., 2021) are used for training and 4405 samples for test. It consists of 2D designs (in a .png format) alongside their mechanical and geometrical constraints. GMCAD's features are detailed in (Almasri et al., 2021)

2.3.2 Geometric Discriminators' Performance

To train the geometric discriminators, we augmented the training dataset with three rotations of 90°, 180°and 270°. The predictive performance of the geometrical discriminators is presented in Fig. 2. In order to evaluate a predictor, an admissible error interval is set (predictions within the green lines in Fig.2 are considered correct). As we can clearly see, the th_{min} predictor shows the highest number of inadmissible predictions (predictions outside the green intervals). To quantify this observation, the percentage of erroneous predictions for every geometrical discriminator is computed.

We choose for the th_{min} and len_{max}lenmax the relative prediction error defined as $e_{\%} = \frac{|True-Predicted|}{True} \times 100$, and for θ_{min} and Nbr_{bars}, $\Delta = |True - Predicted|$. The percentage of predictions that fall within $e_{th_{min}\%} > 5\%$ is 46%, $e_{len_{max}\%} > 5\%$ is 1% , $\Delta\theta_{min} > 5^{\circ}$ is 3,15% and $\Delta Nbr_{bars} > 1\ bar$ is 0,15%. Consequently, we can

conclude that all geometric discriminators are sufficiently precise except for the th_{min} one, which needs further improvement. In fact, if we tolerate a higher error interval of 10% for th_{min}, we would end up with 29,1%of inadmissible predictions

2.3.3 Dl-AM-TO's Performance

Figure 3 shows a sample of real versus generated designs alongside their skeletons and the geometrical metrics: $\Delta\theta_{min}$, ΔNbr_{bars}, and $e_{len_{max}\%}$. In fact, designers are more interested in the design's geometry, which is best defined by the skeletons, which explains their use here for comparison.

Real Design						
Generated Design						
Real Skeleton	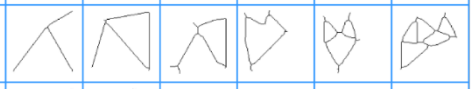					
Generated Skeleton						
ΔNbr_{bars}	0	0	0	0	0	0
$\Delta\Theta_{min}$	-9°	0°	-1°	+4°	+0.5°	0°
$e_{len_{max}\%}$	3.5%	2.9%	0%	7.7%	3.7%	0%
$SSIM$	0.44	0.57	0.55	0.59	0.56	0.58
$SSIM_{skeleton}$	0.7	0.73	0.63	0.76	0.75	0.66

Figure 3: Comparison between the real and generated designs in their full and skeleton formats on the test set.

As we can clearly see, DL-AM-TO captures the geometrical information; $\Delta Nbr_{bars} = 0$, $\Delta\theta_{min}$ rarely exceeds 5°, similarly, $e_{len_{max}\%}$ does not exceed 10%. Aesthetically, the generated designs' skeletons are similar to the real ones; we used the structural similarity index (SSIM) to compare them (Wang et al., 2004). SSIM is ≈ 0.7. The overall geometrical performance was evaluated manually over a sample of 100 designs of the test set; in other terms, we counted the Nbr_{bars} and measured the len_{max}, and θ_{min} manually. We define a design complying with (i) the Nbr_{bars} constraint if $\Delta Nbr_{bars} \leq 1$, (ii) the len_{max} constraint if $e_{len_{max}\%} \leq 10\%$, and (iii) the θ_{min} constraint if $\Delta\theta_{min} \leq 5\%$. We find that 83% of the designs respect the Nbr_{bars} constraint, 76% comply with the len_{max} constraint, and 90% with the θ_{min} constraint.

In order to further investigate the geometrical understanding of DL-AM-TO, we realized the following experiment: We fixed the mechanical constraints and altered one geometrical variable at a time (len_{max} and θ_{min}). To calibrate the design's geometry, we simply need to modify the input value of the de-sired geometrical condition. As we can see, every time we increase len_{max}/θ_{min}, the design's shape is modified in order to comply with this variation while always conforming with mechanical constraints (the *F* and *BC*). However, we can notice that some geometrical constraints are correlated; increasing the θ_{min} alters the len_{max}, and at a certain value, an additional bar appears.

To sum up, DL-AM-TO captures the geometrical and mechanical constraints concurrently and responds to geometrical changes creatively; the obtained results encourage the further improvement of the model

2.3.4 Discussion

The performance of DL-AM-TO relies on several factors. In this study, the traditional SIMP method was used to create the GMCAD dataset for training, with the main objective being the integration of mechanical and geometrical conditions through DL architectures, rather than developing a new TO algorithm. The performance of geometrical discriminators is a key consideration. These discriminators, trained within GAN frameworks, are sensitive to oscillating losses, particularly with the "th_{min}" variable, which, when integrated into the model, resulted in performance deterioration. The "th_{min}" discriminator struggled with precision due to the transformation of CAD designs into image-like representations using computer vision filtering techniques, which can inadvertently change the design's thicknesses.

DL-AM-TO represents a flexible and adaptable approach, as it allows for the incorporation of additional geometric constraints to enhance the generated designs without necessitating significant modifications to the model's architecture. Each input geometric condition can be integrated as an additional objective function of the discriminator. Thus, changing multiple conditions at a time for multiple times will generate a set of optimal Pareto front solutions.

3 DL FOR DATA DRIVEN SHM APPLICATION

Structural Health Monitoring (SHM) is dedicated to the continuous and non-invasive monitoring of structures integrity, ensuring safety and optimal performances through on-site real-time

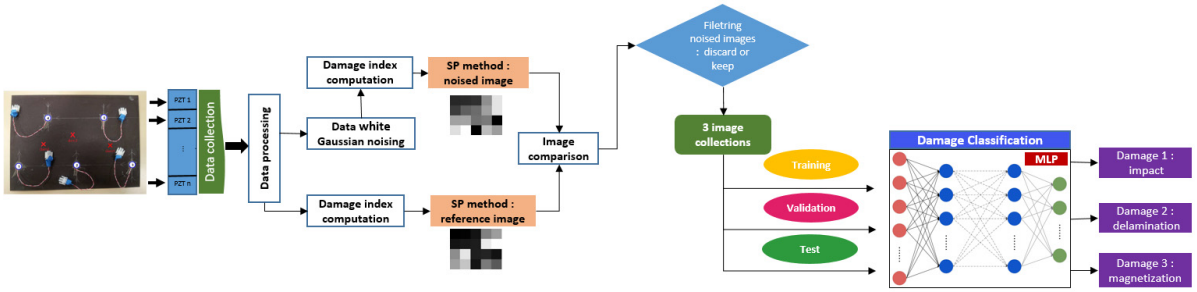

Figure 4: The work dataflow, from data acquisition and transformation into 2D images to MLP classification.

measurements (Worden et al., 2007). Typically, a SHM approach for thin structures relies on the utilization of transducers, such as piezoelectric (PZT), bonded on the structure under examination and that can either send and received ultrasonic waves within the structure to be inspected. Thus, the data collection process associated with the SHM of thin structures using ultrasonic waves generate large datasets composed of many time series associated with all the PT paths available on the structure that need to be processed using robust and efficient techniques in order to determine the presence of the damage and their properties (nature, position, size, etc.). In this study, we investigate new ways of structuring data that increase the accuracy of data driven SHM algorithms and that are based on the physical knowledge related with the structure to be inspected. In particular, the generation of key images from physics-based signals corresponding to all the available PZT paths.

The overall dataflow of the developed SHM algorithm is presented in Figure 4. First, the received signals will be processed to compute the DIs for various tested damage configuration. For each damage case, reference images will then be generated from these DIs, while on the other hand, a white Gaussian noise will be added to the reference signals to compute a new list of DIs. "Noisy" images will then be generated from these noisy DIs and then compared with the reference images in order to keep only images that are relevant for supervised learning. The process is repeated until there are enough images to form image collections for each damage. The images are then separated into training, validation, and test bases depending on the methods, and fed into a MLP to perform a classification task. The methods will finally be compared according to their performance.

3.1 Lamb Waves Raw Data Acquisition

A complex composite aeronautic plate made of composite carbon epoxy is considered (Fig. 5). It is made with 4 plies oriented along [0°/ 45°/ 45°/ 0°] and its dimension are 400x300 mm. A five piezoelectric elements array is used, and each element is bonded to the plate and acts sequentially as sensor and actuator in order to emit and receive Lamb waves signals. They are numbered from 1 to 5 and have a 12.5 mm radius. Three types of damage (impact, delamination, magnet) are considered as shown in Figure 4.

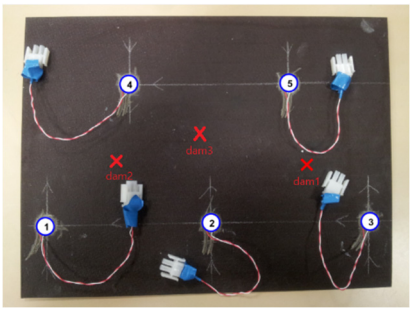

Figure 5: Epoxy plate under study, where "dam1" refers to impact, "dam"2 refers to delamination and "dam3" refers to magnet damage.

The first damage is made by an impact, the second damage is made by placing magnet from both sides of the plate, and the third damage is an artificial delamination achieved by placing a small Teflon tape between two composite plies. Lamb wave measurements were employed for their ability to interact with these damages (Mechbal et., 2017). The signals were 5-cycle bursts with specific parameters, and each signal was collected and emitted with multiple repetitions for statistical robustness. Signal pre-processing included denoising through a discrete wavelet transform and time alignment to account for hardware-induced time misalignments.

Following the collection of signals for all receiver-actuator pairs, a set of 40 candidate Damage Indexes (DIs) designed for damage detection is computed by comparing the damaged state signals with reference signals. The goal was to determine an average score across three sub-scores that assess the

coherence, range, and consistency of these DIs across various scenarios. The study revealed that DIs based on residual energy and signal correlation exhibit the highest robustness, accommodating a wide range of scenarios, environmental conditions, and potential uncertainties, such as variations in the placement of piezoelectric sensors. It's worth noting that for reference-damage configurations, 100 DIs can be generated (comparing 10 healthy signals to 10 damaged ones), whereas for ref-ref comparisons, only 45 DIs are computed due to the exclusion of redundant comparisons within the available repetitions.

3.2 Image Generation from DI's

The developed technique is based on damage index (DI) datasets computed for various damage configurations. It exploits information about the location of piezoelectric transducers (PZTs) to structure a 2D image to match the acquired Lamb wave signals. This approach, called sensor placement (SP), uses the physical positioning of the sensors on the plate, independently of the location of the damage. The image generation process is as follows: in the columns, from left to right, we position the pixels corresponding to the PZT actuator located furthest to the left and right of the plate. The rows of pixels are in the same order as the columns, but this concerns the positions of the receivers. For example, a pixel at coordinates (3,4) in the image matrix characterises the damage index (DI) between the third leftmost PZT, acting as an actuator on the plate, and the fourth leftmost PZT, acting as a sensor. In particular, the actuator positioned in the column is not taken into account, as actuator-receiver pairs involving the same PZT are excluded from the analysis. The available 40 DI's would only provide us with 40 images per damage, which is clearly insufficient for performing supervised deep neural network learning tasks. Therefore, we need to generate more images from the original ones. We chose to use additive white Gaussian noise (AWGN) but in a manner different from what is commonly found in the literature. Indeed, data augmentation techniques often aim to manipulate image support to generate new images. These techniques include flipping, rotation, resizing, cropping, or even adding noise directly to the source image. In our case, it is the temporal signals that are being modified. We add Gaussian noise directly to a signal, stored in our case in matrix. AWGN is characterized by its signal-to-noise ratio (SNR) whose expression is:

$$SNR_{dB} = 10log_{10}\left[\left(\frac{A_{signal}}{A_{noise}}\right)^2\right] = 20log_{10}\left(\frac{A_{signal}}{A_{noise}}\right) \quad (2)$$

Where A_{signal} and A_{noise} represent the amplitudes of the reference signal and the additive noise, respectively.

The AWGN models random noise distributed according to a normal distribution and simulates the background noise, caused for example by interference, of a physical channel, in our case the plate, which serves as an information transmission gateway between a transmitter and a receiver. It is therefore perfectly suited for this kind of situation**.** Signals for the 3 damages that were initially recorded were used to generate 40 reference images that we will call vanilla. At the same time, these signals were then used as a basis for applying AWGN that differ in SNR. A limit SNR above which signal noise does not create images that are sufficiently different from the references was found empirically. Signals are noised with SNRs below the SNR limit and then new DIs are generated and batches of 40 (SP method) noisy images are created per SNR value. Images generated for the SP method with the noisy signals are shown in Figure 6. It can be observed that according to the damage, the reference image and the artificially created AWGN image have the same structure and differ only in the light intensity of some pixel blocks.

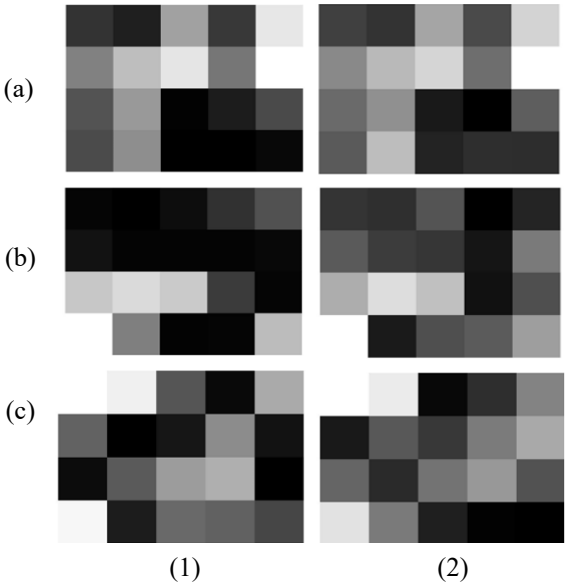

Figure 6: SP vanilla (1) vs. noisy (2) images with AWGN for SNR=50.5 dB and for the DI Welch-based Power Spectral Density (WPSD). Damage is by delamination (a), impact (b) and magnet (c).

The main information in the artificial image, i.e., the white pixel that informs about the largest DI, is

located at the same place and is of the same intensity as in the corresponding vanilla image. After several batches, we finally managed to generate 418 images per class, i.e. 1254 images.

3.3 Classifier Architecture

Deep Learning is increasingly being adopted in the field of Structural Health Monitoring (SHM) (Tabian et al., 2019). In our case, we propose to train a MLP neural network using the SP image dataset that we presented in the previous section. The aim is to use this network to perform a classification of the three types of damage. We have therefore flattened the SP images into a single vector which is used as the input layer of a fully connected hidden MLP. We have proposed a model where the hyper parameters have been finely tuned to obtain the best classification rate. For that, we employed a grid search approach and conducted a series of experiments to systematically determine the optimal hyper parameters of our MLP model. The SOFTMAX activation function at the final layer represents the categorical distribution, assigning scores to each output class and transforming them into probabilities.

3.4 Classification Results

The evaluation of the MLP model's performance will involve analyzing the loss function across epochs. The loss function is a crucial indicator of the model's behavior after each optimization iteration, reflecting its predictive accuracy. Additionally, we will consider the accuracy metric, which measures the model's predictive precision in comparison to the ground truth data. Table 1 summarizes the accuracy and loss results for the proposed MLP model, along with the learning settings applied across multiple training sessions.

Table 1: MLP model classification results.

Total number of images	1254
Number of training data	1003
Number of test images	125
Epochs	30
Learning rate	0.001
Average loss	0.372
Average accuracy	0.928

15 training sessions were conducted for each damage to raise the average information depicted in table 1. When we assess our model performance in classifying the three types of defects, we can see that the results are quite impressive, despite the dataset's size limitations. After training for 30 epochs, the accuracy approaches nearly 1, which means almost perfect classification.

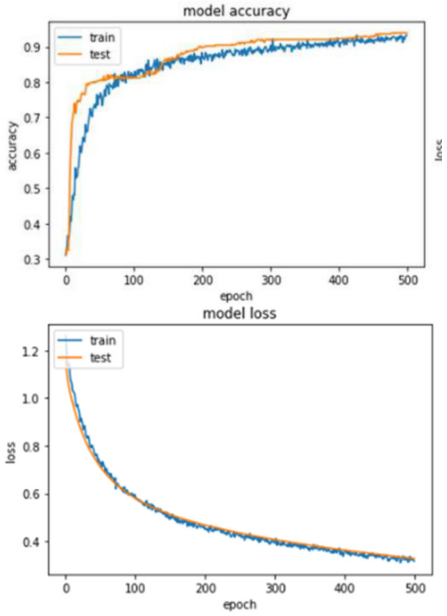

Figure 7: Performance of the MLP model after 500 epochs.

However, we observe a relatively high loss with respect of that high accuracy. This can be understood by examining the loss function mathematically. When we plot a histogram of the loss values for individual samples, it's evident that most samples have very low loss, but a few outliers have significantly higher losses. The MLP results are shown in figure 7. The proposed model performs very well and does not overfit. In fact, the SP images show to fit well for this kind of task that is not too complex. The network manages to class efficiently the three types of damage, with few examples misclassified for the magnet damage as shown in the confusion matrix (figure 8).

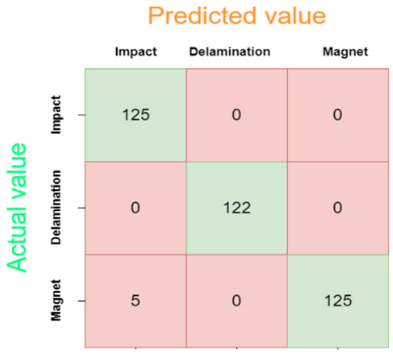

Figure 8: The confusion matrix.

3.5 Discussion

SP images appear to be perfectly suited to the task of classifying defects using an MLP model. Nevertheless, our primary challenge has been the limited availability of data, primarily due to high computational costs. Addressing the issue of data scarcity is a common concern in deep learning. Data augmentation techniques are often employed to artificially expand datasets. Transfer learning, an approach that leverages knowledge gained in solving one problem to address another, is also of interest. While our results suggest that the SP images performs well with limited data, there is potential in exploring how incorporating knowledge from complex neural networks could benefit both methods.

4 CONCLUSIONS

In this paper, we presented two use cases for artificial intelligence in Industry 4.0. The first is an additive manufacturing-driven topological optimisation approach based on deep learning, called DLAM- TO. This technique integrates mechanical and geometric constraints at the same level and generates 2D designs. More interestingly, it easily adapts the geometry of the design to propose several additive manufacturing compliant geometries corresponding to the needs of the design engineer while maintaining a mechanical performance similar to that proposed by SIMP. The second example demonstrated the feasibility of a data-driven approach based on images generated by physics (lamb wave propagation) to classify three types of damage in the context of SHM application. The next step involves finalizing the demonstrators and planning their evaluation by end users, namely, designers and maintenance operators. This phase is crucial to refine these approaches and transform them into fully operational tools intended for use in the context of the factories of the future. It also requires an optimization and adaptation process to ensure their alignment with the specific needs of these professionals before proceeding with the actual deployment in industrial environments.

REFERENCES

Almasri, W., Bettebghor, D., Ababsa, F., Danglade, F. and Adjed, F., 2021, July. Deep Learning Architecture for Topological Optimized Mechanical Design Generation with Complex Shape Criterion. In International Conference on Industrial, Engineering and Other Applications of Applied In-telligent Systems, pp. 222-234, (2021)

Almasri W., Bettebghor D., Adjed F., Ababsa F., Danglade F., GMCAD: an original Synthetic Dataset of 2D Designs along their Geometrical and Mechanical Conditions. In International Conference on Industry 4.0 and Smart Manufacturing, (2021).

Arden, N. S., Fisher, A. C., Tyner, K., Lawrence, X. Y., Lee, S. L., & Kopcha, M.. Industry 4.0 for Pharmaceutical Manufacturing: Preparing for the Smart Factories of the Future. *International Journal of Pharmaceutics*, (2021)

Bendsoe, MP., Kikuchi N., Generating optimal topologies in structural design using a homogenization method, *Computer Methods in Applied Mechanics and Engineering*, vol. 71, no. 2, pp. 197-224, (1988)

Goodfellow, I., Pouget-Abadie, J., Mirza, M., Xu, B., Warde-Farley, D., Ozair, S., Bengio, Y.. Generative adversarial nets. *In: Advances in neural information processing systems*, pp. 2672-2680, (2014)

Khelalef, A., Ababsa, F., Benoudjit, N., An Efficient Human Activity Recognition Technique Based on Deep Learning. Pattern Recognition and Image Analysis 29, 702-715 (2019)

Lockner, Y., Hopmann, C. Induced network-based transfer learning in injection molding for process modelling and optimization with artificial neural networks. *Int J Adv Manuf Technol* **112**, 3501–3513 (2021)

Mechbal, N., Rébillat, M., Damage indexes comparison for the structural health monitoring of a stiffened composite plate. 8th ECCOMAS Thematic Conference on Smart Structures and Materials (SMART 2017) pp. 436-444, (2017)

Mohan, T. R., Roselyn, J. P., Uthra, R. A., Devaraj, D., & Umachandran, K.. Intelligent machine learning based total productive maintenance approach for achieving zero downtime in industrial machinery. *Computers & Industrial Engineering*, (2021)

Nath, A.G., Udmale, S.S. & Singh, S.K. Role of artificial intelligence in rotor fault diagnosis: a comprehensive review. *Artif Intell Rev* 54, 2609–2668 (2021).

Oehlmann, P., Osswald, P., Blanco, J.C. *et al.* Modeling Fused Filament Fabrication using Artificial Neural Networks. *Prod. Eng. Res. Devel.* **15**, 467–478 (2021).

Tabian, I.; Fu, H.; Sharif Khodaei, Z. A Convolutional Neural Network for Impact Detection and Characterization of Complex Composite Structures. Sensors, 19, 4933, (2019)

Wang, Z., Bovik, A.C., Sheikh, H.R. and Simoncelli, E.P., Image quality assessment: from error visibility to structural similarity. IEEE trans-actions on image processing, 13(4), pp.600-612, (2004)

Worden, K.; Farrar, C. R.; Manson, G. & Park, G. "The Fundamental Axioms of Structural Health Monitoring" Proceedings: Mathematical, Physical and Engineering Sciences, The Royal Society, pp. 1639-1664, (2007)

Zhang, Z., Liu, Q.,Wang, Y., Road extraction by deep residual u-net. IEEE Geoscience and Remote Sensing Letters, 15(5), 749-753 (2018).